Published in final edited form as:
Proteins. 2009 February 1; 74(2): 318–327. doi:10.1002/prot.22162.

The First High pH Structure of *Escherichia coli* Aspartate Transcarbamoylase

Kimberly A. Stieglitz[1,*], **Jiarong Xia**[2], and **Evan Kantrowitz**[2]

[1]Department of Chemistry, University of Massachusetts, Boston, MA 02125, USA

[2]Department of Chemistry, Merkert Chemistry Center, Boston College, Chestnut Hill, MA 02467, USA

Abstract

The activity and cooperativity of Escherichia coli aspartate transcarbamoylase (ATCase) vary as a function of pH, with a maximum of both parameters at approximately pH 8.3. Here we report the first X-ray structure of unliganded ATCase at pH 8.5, to establish a structural basis for the observed Bohr effect. The overall conformation of the active site at pH 8.5 more closely resembles the active site of the enzyme in the R-state structure than other T-state structures. In the structure of the enzyme at pH 8.5 the 80's loop is closer to its position in R-state structures. A unique electropositive channel, comprised of residues from the 50's region, is observed in this structure, with Arg54 positioned in the center of the channel. The planar angle between the carbamoyl phosphate and aspartate domains of the catalytic chain is more open at pH 8.5 than in ATCase structures determined at lower pH values. The structure of the enzyme at pH 8.5 also exhibits lengthening of a number of interactions in the interface between the catalytic and regulatory chains, whereas a number of interactions between the two catalytic trimers are shortened. These alterations in the interface between the upper and lower trimers may directly shift the al- losteric equilibrium and thus the coopera- tivity of the enzyme. Alterations in the elec- tropositive environment of the active site and alterations in the position of the cata- lytic chain domains may be responsible for the enhanced activity of the enzyme at pH 8.5.

Keywords

Allosteric regulation; aspartate transcarbamoylase; conformational change; Bohr effect

INTRODUCTION

The Bohr effect was first observed for hemoglobin by Christian Bohr in 1904.[1] Bohr observed that an increase in blood carbon dioxide levels accompanied by a decrease in pH, caused hemoglobin to bind oxygen with less affinity. Today, the Bohr effect more commonly refers to alterations in substrate affinity or enzyme activity as a function of pH, and has been studied extensively in a variety of allosteric proteins and enzymes such as hemoglobin.[2,3]

Correspondence to Kimberly A. Stieglitz, Department of Chemistry, University of Massachusetts Boston, 100 Morrissey Blvd, Boston, MA 02125, kimberly.stieglitz@umb.edu.

Coordinates for the structure of ATCase at pH 8.5 have been deposited in the Protein Data Bank as entry 3D7S.

[1]To distinguish amino acids in the catalytic and regulatory chains of aspartate transcarbamoylase a c (catalytic) or r (regulatory) is appended to the residue number (e.g. Asp236c and Lys143r). To clarify a particular catalytic or regulatory chain, the chain number is also appended to the residue number (e.g. Asp236c4 and Lys143r1).

Escherichia coli aspartate transcarbamoylase (EC 2.1.3.2, ATCase) is an allosteric enzyme whose activity is strongly modulated by pH, exhibiting maximum activity and cooperativity at pH 8.3.[4] The enzyme exhibits homotropic cooperativity for aspartate,5 and is heterotropically regulated by the end-products of the pyrimidine nucleotide pathway CTP,5 as well as, UTP in the presence of CTP.6 ATP, the end-product of the parallel purine pathway, activates the enzyme.[5] In the absence of substrates, the enzyme is predominately in the low-affinity, low-activity T state, whereas the enzyme with both substrates or the bisubstrate analog N-phosphonacetyl-L-aspartate (PALA), is predominately in the high-affinity, high-activity R state.[7] The T to R transition involves an expansion of the molecule by 11 Å along the threefold axis, a rotation of the catalytic subunits by 158 about the molecular threefold axis, and a rotation of the regulatory subunits by 108 about their respective twofold axes.8,9

The active sites of ATCase are shared between adjacent catalytic chains in the trimer.[10–12] On the binding of carbamoyl phosphate (CP) local conformational changes occur, forming the high-affinity binding pocket for Asp due to the repositioning of the 50's loop (residues 50–55) and the movement of the 80's loop (residues 73–88) from the adjacent chain into posi- tion to bind the CP molecule.[13] On the binding of Asp to the enzyme CP complex, the two domains of the cata- lytic chain undergo a domain closure, bringing CP and Asp into close proximity for reaction.14

The influence of pH on ATCase has been studied by analysis of proton binding, substrate binding, and conformational transitions.[15] These studies evaluated the net changes in the state of ionization of the protein and substrate analogues.[15] Isotope trapping studies revealed that at least four ionizable side chains are involved in sub- strate binding and catalysis.[16] Two residues with pKa values of 7 and 9 must be protonated for the binding of CP and Asp, respectively. The catalytically productive form of the enzyme CP complex has a group with a pKa of 7.0 protonated and a group with a pKa of 9.1 deprotonated. When studying the pH effect on the kinetic and regulatory properties of ATCase, Pastra-Landis et al.[4] proposed that there is a residue essential for cooperativity at or near the Asp binding site with a pKa of 8.5. This study also suggested that the pH-dependent shift in the Asp saturation curve is largely because of changes involving intersubunit salt bridges. Finally, a detailed study of the Bohr effect in ATCase was performed using calorimetry, potentiometry, and spectrophotometry to analyze the coupling between the binding of protons and substrate analogues.[15,17] This work identified two residues with pKa values of 6.3 and a third residue with a pKa of 9.1 that play a critical role in the Bohr effect of ATCase.[18]

Extensive studies of the three-dimensional structure of E. coli ATCase at low pH (5.9) in the presence and absence of substrate/substrate analogues have been reported,[8,19,20] as well as additional structural studies of the enzyme at pH 7.2[1–24] However, no structure of the unliganded enzyme has been determined at a pH where the enzyme exhibits maximal activity and cooperativity (pH 8.3), due to difficulties in crystallizing the enzyme under these conditions. Here, we report the first X-ray structure of unliganded *E. coli* ATCase at pH 8.5. These data shed light on the structural basis for how alterations in pH influence the catalysis and cooperativity of the enzyme.

Materials and Methods

Materials

Agar, ampicillin, 2-mercaptoethanol, polyethyleneglycol 4000, potassium dihydrogen phosphate, sodium ethylenediaminetetracetic acid, sodium acetate, uracil were obtained from Sigma Chemical Co. (St. Louis, MI). Q-Sepharose Fast Flow resin was obtained from Amersham Pharmacia Biosciences. Casamino acids, yeast extra and tryptone were obtained

from Difco (Detroit, MI). Sodium dodecyl sulfate was purchased from Bio-Rad Laboratories. Enzyme grade ammonium sulfate, Tris, electrophoresis grade acrylamide, agarose, were purchased from ICN Biomedicals (Costa Mesa, CA). Crystal cryo-mountig loops and siliconized cover slides were obtained from Hampton Research (Laguna Niguel, CA).

Methods

Expression and purification of the enzyme—*E. coli* ATCase was overexpressed utilizing strain EK110425 containing the plasmid pEK152.26 The overexpression, isolation, and purification of the enzyme were performed as described previously.[25] The concentration of enzyme was determined by absorbance measurements at 280 nm with an extinction coefficient of 0.59 $(mg/ml)^{-1}$ cm^{-1}.[27] The purity of the enzyme was checked by SDS-PAGE[28] and nondenaturing PAGE.[29,30]

Crystallization and freezing of crystals—ATCase was crystallized by the hanging drop vapor dif- fusion. The enzyme solution, at 10 mg/mL, was mixed 50%/50% (v/v) with a solution of crystallization buffer (100 mM Tris, 200 mM Li_2SO_4, 25% PEG3300 (w/v) pH 8.5), and then equilibrated against 1 mL of crystallization buffer. Crystals grew to average dimensions of $0.3 \times 0.3 \times 0.1$ mm^3 within 5 weeks. Crystals were transferred into a cryoprotectant composed of 20% glycerol in crystallization buffer for ~1 min before the crystals were frozen in liquid nitrogen.

X-ray data collection and processing—The data for the structure in the ATCase were collected using a Rigaku R-axis IV++ detector while X-rays were generated using a Rigaku RU-200 rotating-anode generator operating at 50 kV and 100 mA at the Crystallographic Facility in the Chemistry Department of Boston College. The diffraction data were integrated, scaled and averaged using HKL2000.[31]

Structural Refinement—The initial model for the high pH structure was derived from the coordinates of a mutant version of ATCase (K244N) (PDB code 1SKU) which crystallized at pH 7 in the same space group (H3) and with similar unit cell dimensions (a = b = 125.67 c = 198.20).[32] Before refinement with CNS,33 all the waters and ligands were removed. After initial rigid body, simulated annealing, minimization, and B-factor refinement the initial maps were inspected. The 80's loop of the catalytic chain was found to be disordered. Several rounds of manual rebuilding, using XtalView34 and refinement were performed to correct the structure.

Waters were added to the structure on the basis of Fo - Fc electron density maps at or above the 2.5σ level using COOT[35] and subsequently refined with REFMAC.[36] Waters were retained only when they could be justified by hydrogen bonds. The model was checked for errors using PROCHECK.[37] The details of data collection, processing, and refinement are provided in Table I.

Method of calculating pKa's of residues—Residue pK_a values were calculated using MCCE[38] which utilizes Delphi as the Poisson-Boltzmann equation solver.[39] To include all residues in the shared active site, the calculations were performed on the combination of one C1 and one C2 catalytic chain. The MCCE program was run in quick mode with the dielectric constant of the protein set to four. Analysis of the final conformation of the protein side chains of the T_{low_apo} and the $T_{high\ apo}$ structures revealed that the side chains of active site residues varied less than 1.5 Å from their original positions.

RESULTS AND DISCUSSION

The study presented here examines how pH influences the structure of ATCase and to what degree this is responsible for the observed Bohr effect of ATCase. The most noticeable effect of pH on the function of ATCase is that the activity of the enzyme increases dramatically as the pH increases from 6.1 to 8.8. The maximal observed velocity of ATCase at pH 8.8 is almost 11-fold higher than the maximal velocity at pH 6.1.[4] In addition to this dramatic increase in activity, ATCase lacks cooperativity at low pH (Hill coefficient = 1 at pH 6.14). Cooperativity increases as a function of pH with the Hill coefficient attaining a maximal value at pH ~8.5.[4]

Three-dimensional structure of E. coli ATCase at pH 8.5

ATCase crystallized at pH 8.5 in the space group H3 rather than the more common P321 space group observed for ATCase crystals. The unit cell dimensions of the crystals of ATCase grown at pH 8.5, in the H3 space group, T_{high_apo}, (a = b = 129.78 A, c = 197.74 A) are similar to the unit cell dimensions of the few other T- state crystals of ATCase in the H3 space group. Two of these structures in the H3 space group are of the wild- type enzyme with substrates or substrate analogs in the active site (PDB entries: 1ROC24 and 2AIR40), whereas two were for the P268A (PDB entry 1EZZ41) and the K244N (PDB entry 1SKU32) mutant versions of ATCase in the absence of substrates or substrate analogues. The similarity of the unit cell dimensions of the T_{high_apo} crystals reported here, as compared with these known T- state structures in the same space group grown at pH values of seven or less, suggested that the crystals grown at pH 8.5 were in the T-quaternary structure. Therefore, the initial model used for the refinement of the structure was the T-state structure of the K244N mutant ATCase in the H3 space group (PDB code 1SKU).[32] The data for the T_{high_apo} were refined to a R_{factor} and R_{free} of 21.5% and 24.7%, respectively, with 213 water molecules in the asymmetric unit.

Quaternary structure

To evaluate the quaternary structure of the enzyme, the vertical separation along the threefold axis between the center of mass of the upper and lower catalytic subunits were determined and compared with previously determined structures of ATCase in the T and R states. The vertical separation for ATCase in the T and R states was 45.6 Å and 56.6 Å, respectively.[42] The difference between the R- and T-state vertical separations corresponds to the vertical expansion of the enzyme observed in the T to R transition (56.6 − 45.6 = 11 Å). For the T_{high_apo} structure the vertical separation was 45.2 Å, similar to the vertical separation of the T state of the enzyme determined at other pH values. These data indicate that the T_{high_apo} structure reported here is in the T-quaternary conformation.

Tertiary structure of the catalytic chain of ATCase at high pH

To better understand the influence of pH on the homotropic cooperativity of ATCase the catalytic chains in the T_{high_apo} structure were compared, after superposition with CNS,33 to the catalytic chains of the T_{low_apo} and R_{low_pala} structures (see Fig. 1). The RMS deviation of the α-carbon atoms between the C1 catalytic chain of the T_{high_apo} and T_{low_apo} structures was 1.33 Å . Shown in Figure 1(A) is the structure of one catalytic chain (C1) with the portion of the 80's loop of the adjacent catalytic chain (C2) that donates residues into the active site. On the tertiary level, the two structures are very similar with the exception of the 80's loop from residues 73 to 88 (C1 and C2) and a small region of the 240's loop, which are both clearly different.

Shown in Figure 1(B) is a similar comparison between the T_{high_apo} and R_{low_pala} structures. The RMS deviation of the α-carbon atoms between the C1 catalytic chain of the T_{high_apo}

and R_{low_pala} structures was 2.61 Å. The region that shows the largest difference between the two structures is the 240's loop. These data indicate that the tertiary structure of the catalytic chains of the T_{high_apo} structure are in a T-like conformation. However, in the T_{high_apo} structure the 80's loop, which is critical for the initiation of the T to R transition, is in a significantly different position than in the T_{low_apo} structure [Fig. 1(A)]. The overall RMS deviation including both α-carbon and side chain atoms between the 80's loop of the T_{high_apo} catalytic chain and the R_{low_pala} and T_{low_apo} structures were 5.58 Å and 4.69 Å, respectively, whereas the corresponding RMS deviation between the T_{low_apo} and R_{low_pala} structures was 11.45 Å [Fig. 1(C)]. The B-factors for the 80's loop residues in the T_{high_apo} struc-ture are similar to those in other structures determined at lower pH. The conformation of the 80's loop in the T_{high_apo} structure is also closer to $R_{neutral\_pala}$ structure than to the $T_{neutral\_ca}$ structure. In addition to a major alteration in the position of the 80's loop, there are also smaller but significant alterations in portions of the 50's and 240's loops. These loop alterations may account for changes in substrate affinity and activity, since the 50's and 80's loops are involved in the binding of CP and the 80's and 240's loops are involved in the binding of Asp.

Tertiary structure of the regulatory chain of ATCase at high pH

To further understand how pH can influence the properties of ATCase, the T_{low_apo}, and the T_{high_apo} regulatory chains were compared. The RMS deviation of α-carbons of the T_{high_apo} and the T_{low_apo} regulatory chain was 2.8 Å. There were some small but significant differences in the tertiary structure between the two structures in the 50r's loop and in the 130r's loop of the regulatory chains. The electrostatics in the region around Arg130r, Asn132r, and Asp133r of the T_{high_apo} structure exhibited large shifts compared with structures determined at lower pH values. The differences in the 50r's region are due to changes in the architecture of the allosteric binding site. More specifically, a comparison of the allosteric binding site of the T_{high_apo} and T_{low_apo} structures revealed that there is a hydrogen-bonding network present in the Thigh_apo structure that is not present in the T_{low_apo} structure. Residues Asp19r, His20r, Ser50r, and Lys56r are engaged in a hydrogen-bonding network in the T_{high_apo} structure with the side chain of nearby Glu52r. His20r in the T_{low_apo} structure interacts only with the backbone of Glu52r and Lys56r, but does not interact with Asp19r or Ser50r as observed in the T_{high_apo} structure. In the T_{low_apo} structure, Lys56r only interacts with Asp19r. The interactions involving Lys56r in the T_{high_apo} structure can be used to help explain the important functional role of this residue.[45]

As opposed to most structures of the enzyme at low pH, the N-terminus (residues 1r–13r) of the T_{high_apo} structure was well defined in electron density maps at 1.8σ and appeared to be in a unique conformation that may influence the binding of ATP and CTP, as more hydrogen bonding donors are facing inward toward the phosphate binding pocket.

The active site of the Thigh_apo structure

The 2Fo - Fc electron density map of the C1 active site of the T_{high_apo} structure is shown in Figure 2(A). The side chains in the active site were well ordered even though there was no substrate or substrate analogues present. The active site of the T_{high_apo} structure is more similar to the active site in the R state, than any other T-state structures. As comparison of the T_{low_apo} structure there where significant changes in the side chain positions of Arg105, Arg229, Lys232, as well as residues of the adjacent 80's loop. To better understand the positional changes that occur to accommodate substrate binding, the $T_{low\_CTP\_CP}$ structure was compared with the T_{high_apo} structure. The conformation of the 50's loop region of the T_{high_apo} structure, as compared with the $T_{low\_CTP\_CP}$ structure [Fig. 2(B)] ideally positions the CP domain to interact with the carbonyl oxygen and nitro- gen of CP. More specifically, the distance from the carbonyl oxygen of CP to the nitrogen H-donor of Arg54 was 0.8 Å

less in the T_{high_apo} as compared with the $T_{low\_CTP\_CP}$ structure. The same structural comparison revealed that the distance from Arg105 to both the phosphate oxygen and carbonyl oxygen was 0.6 Å less. In contrast, Ser52, Thr53, and Thr55 as well as Ser80 from the adjacent catalytic chain were in different conformations in the T_{high_apo} and $T_{low\_CTP\_CP}$ structures [Fig. 2(B)]. The T_{low_apo} was also compared with the T_{high_apo} structure and both the 80's and 50's regions were in different conformations. The T_{high_apo} structure is not intermediate between the $T_{low_CTP_C}$P and T_{low_apo} structures, but rather is in a unique conformation.

To evaluate the electrostatics of the active site, the electrostatic potentials mapped onto the molecular surface of T_{high_apo}, T_{low_apo}, and $T_{low\_CTP\_CP}$ structures were compared. As seen in Figure 3(A), the T_{high_apo} structure has a unique positively charged "cleft" or "channel" consisting of residues from the 50's region with Arg54 positioned in the center of the channel. In the T_{high_apo} structure, the previously seen T-state stabilizing interaction between Arg54c1* and Glu86c2 is not observed. In the T_{high_apo} structure, Arg54 forms an interaction with Ser52, stabilizing the observed alternate conformation of the 50's region, and an interaction with Asn78c2 stabilizing the observed alternate conformation of the 80's loop [Fig. 4(A)].

For comparison, Figure 3(B) shows the electrostatic potential mapped on the molecular surface of the T_{low_apo} structure. The CP domain portion of the active site in the T_{high_apo} structure is much more electropositive than the corresponding portion of the active site of the T_{low_apo} structure. In addition, the 50's region is in a more closed conformation in the T_{low_apo} structure as compared with the T_{high_apo} structure [compare Fig. 3(A,B)]. In the case of the $T_{low\_CTP\_CP}$ structure, both the CP and Asp domain exhibit a diminished positive electrostatic surface potential as compared with the T_{high_apo} structure. However, in the $T_{low\_CTP\_CP}$ structure, the CP and Asp domains are in a more closed conformation than the T_{high_apo} and T_{low_apo} structures [compare Fig. 3(C) with Fig. 3(A,B)]. The difference in the electrostatics of the active site of ATCase between the structures determined at low and high pH is induced by the observed local conformational changes of both the 50's and the 80's loops. Upon the binding of CP, the 50's region undergoes structural alterations that are critical for the formation of the high-activity, high-affinity Asp binding site.[13] The positive electrostatic environment of the active site will promote neutralization of negatively charged CP on binding and make the phosphate a better leaving group. It is tempting to speculate that the electropositive channel observed in the T_{high_apo} structure provides a path for easy entry of CP into the active site. Since the catalytic activity of the enzyme is highly dependent on Arg54,[49,50] the repositioning of the Arg54 side chain may contributes to the Bohr effect of ATCase.

The structural effect of pH on the active site architecture as observed in the T_{high_apo} structure is shown in Figure 4. In the T_{high_apo} structure, there is a unique hydrogen-bonding network involving residues Arg105, Thr55, Ser52, Arg54, and Asn78 of the 80's loop of the adjacent chain [Fig. 4(B)]. Such an intricate hydrogen- bonding network is not observed in other ATCase structures determined at lower pH [see Fig. 4(A)]. In the Asp domain of the T_{high_apo} structure, there is a hydrogen-bonding network involving residues Gln231, Arg229, Lys232, Asp271, Tyr240, and Lys84 of the adjacent catalytic chain [Fig. 4(B)] that is not observed in the T_{low_apo} structure [Fig. 4(A)]. The interactions observed in the active site of the T_{high_apo} structure are similar to those observed in the R-state structure of the enzyme bound with an analogue of CP, phosphonoacetylamide (R_{D236_PAM}).[51] These observations further support the notion that the active site of the Thigh_apo structure has certain characteristics of the R-state structure.

The position of 80's loop, stabilized by interactions between Lys232c1 and Lys84c2 as well as between Arg54c1 and Asn78c2, in the T_{high_apo} structure con- tributes to a more open conformation of the active site cavity [Fig. 4(B)], rendering the active site cavity more solvent accessible. The enhanced electropositive environment of the active site in the T_{high_apo} structure (see Fig. 3) also provides a more complementary electrostatic interaction for CP.

Relative positions of the catalytic chain domains

The planar angle[52] between the CP and Asp domains was determined to quantify and compare the degree of openness of the active site of the T_{high_apo} structure relative to the active sites of other T-state and R-state structures. The planar angles between the CP and Asp domains of the T_{high_apo} structure were 139.38 and 137.58 for the C1 and the C6 catalytic chains, respectively. In contrast the planar angles between the CP and Asp domains of the T_{low_apo} structure are more closed, with angles of 135.78 and 134.18 for the C1 and C6 chains, respectively. Since these planar angles are calculated using the center of mass of the two domains and a hinge point (α-carbon of residue 140), differences larger than 18 are significant. The planar angles between the CP and Asp domains of the $T_{low\_CTP\_CP}$ structure were also more closed than in the T_{high_apo} structure (133.48 and 135.28 for the C1 and C6 chains, respectively). In addition, the product bound T structure, $T_{neutral\_ca}$, has planar angles between the CP and Asp domains of 137.58 and 137.48 for the C1 and C6 chains, respectively, which is a more closed conformation than observed in the T_{high_apo} structure. In summary, the two domains of the catalytic chain in the T_{high_apo} structure are in a more open conformation than in any other structure at lower pH values. A more open conformation may not necessarily promote higher affinity, but the more positive electrostatic environment observed, combined with the increased solvent accessibility, may pro- vide better access of CP to the active site cavity.

Alterations in interchain interactions

To understand how changes in pH influence the inter- chain interactions of ATCase, the C1–R1 and C1–C4 interchain interactions of the T_{high_apo} and T_{low_apo} structures were compared. Most of the C1–R1 interactions were further apart in the T_{high_apo} structure than the corresponding interactions in the T_{low_apo} structure. For example, the interaction between Pro107c1 and Asn113r1 increased from 3.0 Å in the T_{low_apo} to 3.5 Å in the T_{high_apo} structure. The interaction between Glu109c1 and Asn113r1 increased from 3.0 Å in the T_{low_apo} to 3.6 Å in the T_{high_apo} structure and the interaction between Ser131c1 and Lys143r1 increased from 2.7 Å in the T_{low_apo} to 3.1 Å in the T_{high_apo} structure. A new interaction was also observed in the T_{high_apo} structure between Gln133c and Glu142r.

As opposed to the increase in distance of the interactions between the C1–R1 chains, the interchain interactions between the C1–C4 chains at high pH are shorter by 0.5–0.6 Å compared with the length of these interactions in the low pH structures. For example, the critical T-state stabilization interaction between Glu239c1 and both Tyr165c4 and Lys164c4 are both 2.65 Å in T_{high_apo} structure, compared with 3.17 Å and 3.24 Å in the T_{low_apo} structure. The shorter distances of these C1–C4 interactions suggest that they are stronger and that at high pH the T-state of the enzyme is more stable than at lower pH. The enhanced stabilization of the T-state at high pH may be responsible for the higher observed cooperativity.

Calculation of pKa values

The MCCE[38] program was used to investigate alterations in pK_a values because of the structural changes between the T_{low_apo} and the T_{high_apo} structures. Within the active site area there were significant shifts in pK_a values (>1.0 pK_a units) for four residues: His134c1,

Lys232c1, Lys84c2, and Glu86c2 (see Table II). His134 has been proposed to act as a base accepting a proton from the amino group of Asp.[53] When His134 is replaced by Ala, the mutant enzyme exhibits a 20-fold reduction in activity as compared with the wild-type enzyme. In the T_{high_apo} structure, His134 is observed to help create the positive electrostatic channel in the "R-like" active site. The MCCE[38] calculations suggest that the pK_a of His134 is 1.8 units higher in the T_{high_apo} as compared with the T_{low_apo}. This increase would enhance the ability of His134 to accept protons. The pK_a of Glu86 in the T_{high_apo} structure was 8.5, 3.5 units higher than in the T_{low_apo} structure. This higher pK_a is within the pKa range of the group that must be protonated for binding of the substrates.[16] The structural basis for this may be due to the formation of a salt link between Glu86c2 with Arg54c1. Also, the pK_a of Lys84c2 decreases by 2.5 units and the pK_a of Lys232c1 increases by 1.9 units. The decrease in the pK_a of Lys84c2 supports the previous suggestion that this residue may act as a base accepting a proton from the tetrahedral intermediate.[54] The alterations in the pKa values of these two Lys residues also have a dramatic effect on the shape of the Asp binding pocket [compare Fig. 3(B,C)].

SUMMARY

Analysis of the T_{high_apo} structure demonstrates that the pH influences homotropic cooperativity by strengthening the interactions between the interface between the upper and lower catalytic trimers (e.g., the C1–C4 interface and the symmetry related interfaces) and thereby shifting the allosteric equilibrium toward the T state. Analysis of the structure also suggests that the enhanced catalytic activity of the enzyme at pH 8.5 may be because of the observed alterations in the electrostatics of the active site as well as a more open conformation of the two domains of the catalytic chain. pH also influences the interactions between the catalytic and regulatory chains which could be responsible for the observed changes in heterotropic properties of the enzyme as a function of pH. To fully understand how the structural changes due to alterations in pH influence the homo- tropic and heterotropic properties of ATCase an X-ray structure of the enzyme in the R state at high pH would be extremely useful.

Acknowledgments

Grant sponsor: National Institutes of Health, Grant number GM26237

Abbreviations

ATCase	*Escherichia coli* aspartate transcarbamoylase holoenzyme
CP	carbamoyl phosphate
Asp	L-aspartate
PAM	phosphonacetamide
PALA	N-phosphonacetyl-L-aspartate
CA	N-carbamoyl-L-aspartate
C1/C6	the two catalytic chains of ATCase in the asymmetric unit of the crystal
R1/R6	the two regulatory chains of ATCase in the asymmetric unit of the crystal
C/R	the catalytic and regulatory chain interface
T_{high_apo}	the T-state X-ray structure of unliganded ATCase determined at pH 8.5 and reported here

T_{low_CTP}	the T-state X-ray structure of ATCase in the presence of CTP determined at pH 5.8 (PDB code 1ZA1)
$T_{low\_CTP\_CP}$	the T-state X-ray structure of ATCase in the presence of both CTP and CP determined at pH 5.8 (PDB code 1ZA2)
T_{low_apo}	the T-state X-ray structure of unliganded ATCase determined at pH 5.8 (PDB code 6AT1)
R_{low_pala}	the R-state X-ray structure of ATCase in the presence of PALA determined at pH 5.8 (PDB code 1D09)
$T_{neutral\_ca}$	the T-state X-ray structure of ATCase in the presence CA and phosphate determined at pH 7.0 (PDB code 1R0C)
$R_{neutral\_pala}$	the R-state X-ray structure of ATCase in the presence of PALA determined at pH 7.0 (PDB code 1Q95)
RMS	root mean square

REFERENCES

1. Bohr C. Uber den einfkuss der kohlensauerspannung auf die sauer- stof-faufnahme im blute. Zbl Physiol 1904;17:661.
2. Perutz MF, Kilmartin JV, Nishikura K, Fogg JH, Butler PJ, Rollema HS. Identification of residues contributing to the Bohr effect of human haemoglobin. J Mol Biol 1980;138:649–668. [PubMed: 7411620]
3. Perutz MF, Muirhead H, Mazzarella L, Crowther RA, Greer J, Kil- martin JV. Identification of residues responsible for the alkaline Bohr effect in haemoglobin. Nature 1969;222:1240–1243. [PubMed: 5789657]
4. Pastra-Landis SC, Evans DR, Lipscomb WN. The effect of pH on the cooperative behavior of aspartate transcarbamylase from Escherichia coli. J Biol Chem 1978;253:4624–4630. [PubMed: 26686]
5. Gerhart JC, Pardee AB. Enzymology of control by feedback inhibi- tion. J Biol Chem 1962;237:891–896. [PubMed: 13897943]
6. Wild JR, Loughrey-Chen SJ, Corder TS. In the presence of CTP, UTP becomes an allosteric inhibitor of aspartate transcarbamylase. Proc Natl Acad Sci USA 1989;86:46–50. [PubMed: 2643106]
7. Hervé G, Moody MF, Tauc P, Vachette P, Jones PT. Quaternary structure changes in aspartate transcarbamylase studied by X-ray solution scattering; signal transmission following effector binding. J Mol Biol 1985;185:189–199. [PubMed: 3900420]
8. Ke H-M, Lipscomb WN, Cho Y, Honzatko RB. Complex of N-phosphonacetyl-L-aspartate with aspartate carbamoyltransferase: X-ray refinement, analysis of conformational changes and catalytic and allosteric mechanisms. J Mol Biol 1988;204:725–747. [PubMed: 3066911]
9. Krause KL, Voltz KW, Lipscomb WN. 2.5 Å structure of aspartate carbamoyltransferase complexed with the bisubstrate analog N- (phosphonacetyl)-L-aspartate. J Mol Biol 1987;193:527–553. [PubMed: 3586030]
10. Krause KL, Voltz KW, Lipscomb WN. Structure at 2.9-Å resolution of aspartate carbamoyltransferase complexed with the bisubstrate analogue N-(phosphonacetyl)-L-aspartate. Proc Natl Acad Sci USA 1985;82:1643–1647. [PubMed: 3856843]
11. Monaco HL, Crawford JL, Lipscomb WN. Three-dimensional structures of aspartate carbamoyltransferase from Escherichia coli and of its complex with cytidine triphosphate. Proc Natl Acad Sci USA 1978;75:5276–5280. [PubMed: 364472]
12. Robey EA, Schachman HK. Regeneration of active enzyme by formation of hybrids from inactive derivatives: implications for active sites shared between polypeptide chains of aspartate transcarbamoylase. Proc Natl Acad Sci USA 1985;82:361–365. [PubMed: 3881763]

13. Wang J, Stieglitz KA, Cardia JP, Kantrowitz ER. Structural basis for ordered substrate binding and cooperativity in aspartate transcarbamoylase. Proc Natl Acad Sci USA 2005;102:8881–8886. [PubMed: 15951418]

14. Wang J, Eldo J, Kantrowitz ER. Structural model of the R state of Escherichia coli aspartate transcarbamoylase with substrates bound. J Mol Biol 2007;371:1261–1273. [PubMed: 17603076]

15. Knier BL, Allewell NM. Calorimetric analysis of aspartate transcarbamylase from Escherichia coli. Binding of substrates and substrate analogues to the native enzyme and catalytic subunit. Biochemistry 1978;17:784–790. [PubMed: 343809]

16. Turnbull JL, Waldrop GL, Schachman HK. Ionization of amino acid residues involved in the catalytic mechanism of aspartate transcarbamoylase. Biochemistry 1992;31:6562–6569. [PubMed: 1633167]

17. Allewell NM, Friedland J, Niekamp K. Calorimetric analysis of aspartate transcarbamylase from Escherichia coli: binding of cytosine 50-triphosphate and adenosine 5'-triphosphate. Biochemistry 1975;14:224–230. [PubMed: 235271]

18. Allewell NM, Hofmann GE, Zaug A, Lennick M. Bohr effect in Escherichia coli aspartate transcarbamoylasse. Linkage between substrate binding, proton binding, and conformational transitions. Bio- chemistry 1979;18:3008–3015.

19. Jin L, Stec B, Lipscomb WN, Kantrowitz ER. Insights into the mechanism of catalysis and heterotropic regulation of E. coli aspartate transcarbamoylase based upon a structure of enzyme complexed with the bisubstrate analog N-phosphonacetyl-L-aspartate at 2.1 Å. Proteins: Struct Funct Genet 1999;37:729–742. [PubMed: 10651286]

20. Ke H-M, Honzatko RB, Lipscomb WN. Structure of unligated aspartate carbamoyltransferase of Escherichia coli at 2.6-Å resolution. Proc Natl Acad Sci USA 1984;81:4027–4040.

21. Gouaux JE, Lipscomb WN. Crystal structures of phosphonoacetamide ligated T and phosphonoacetamide and malonate ligated R states of aspartate carbamoyl-transferase at 2.8 Å resolution and neutral pH. Biochemistry 1990;29:389–402. [PubMed: 2405902]

22. Gouaux JE, Stevens RC, Lipscomb WN. Crystal structures of aspartate carbamoyl-transferase ligated with phosphonoacetamide, malonate and CTP or ATP at 2.8 Å resolution and neutral pH. Biochemistry 1990;29:7702–7715. [PubMed: 2271529]

23. Huang J, Lipscomb WN. Products in the T-state of aspartate transcarbamylase: crystal structure of the phosphate and N-carbamyl-L-aspartate ligated enzyme. Biochemistry 2004;43:6422–6426. [PubMed: 15157076]

24. Huang J, Lipscomb WN. Aspartate transcarbamylase (ATCase) of Escherichia coli: a new crystalline R-state bound to PALA, or to product analogues citrate and phosphate. Biochemistry 2004;43:6415–6421. [PubMed: 15157075]

25. Nowlan SF, Kantrowitz ER. Superproduction and rapid purification of E. coli aspartate transcarbamoylase and its catalytic subunit under extreme derepression of the pyrimidine pathway. J Biol Chem 1985;260:14712–14716. [PubMed: 3902838]

26. Baker DP, Kantrowitz ER. The conserved residues glutamate-37, aspartate-100 and arginine-269 are important for the structural stabilization of Escherichia coli aspartate transcarbamoylase. Biochemistry 1993;32:10150–10158. [PubMed: 8104480]

27. Gerhart JC, Holoubek H. The purification of aspartate transcarbamylase of Escherichia coli and separation of its protein subunits. J Biol Chem 1967;242:2886–2892. [PubMed: 5338508]

28. Laemmli UK. Cleavage of structural proteins during the assembly of the head of bacteriophage T4. Nature 1970;227:680–685. [PubMed: 5432063]

29. Davis BJ. Disc electrophoresis-II method and application to human serum proteins. Ann N Y Acad Sci 1964;121:404–427. [PubMed: 14240539]

30. Ornstein L. Disc electrophoresis. I. Background and theory. Ann N Y Acad Sci 1964;121:321–349. [PubMed: 14240533]

31. Otwinowski, Z.; Minor, W. Processing of X-ray diffraction data collected in oscillation mode. In: Carter, CW., Jr; Sweet, RM., editors. Methods enzymol. Vol. Vol. 276. New York: Academic Press; 1997. p. 307-326.

32. Alam N, Stieglitz KA, Caban MD, Gourinath S, Tsuruta H, Kantro- witz ER. 240's loop interactions stabilize the T state of Escherichia coli aspartate transcarbamoylase. J Biol Chem 2004;279:23302–23310. [PubMed: 15014067]
33. Brünger AT, Adams PD, Clore GM, DeLano WL, Gros P, Grosse-Kunstleve RW, Jiang J-S, Kuszewski J, Nilges N, Pannu NS, Read RJ, Rice LM, Simonson T, Warren GL. Crystallography and NMR system (CNS): a new software system for macromolecular structure determination. Acta Crystallogr D 1998;54:905–921. [PubMed: 9757107]
34. McRee DE. Xtalview/Xfit—a versatile program for manipulating atomic coordinates and electron density. J Struct Biol 1999;125:156–165. [PubMed: 10222271]
35. Emsley P, Cowtan K. Coot: model-building tools for molecular graphics. Acta Crystallogr D 2004;60(Part 12 Part 1):2126–2132. [PubMed: 15572765]
36. Murshudovv GN, Vagin AA, Dodson EJ. Refinement of macromolecular structures by the maximum-likelihood method. Acta Crystallogr D 1997;53:240–255. [PubMed: 15299926]
37. Laskowski RA, MacArthur MW, Moss DS, Thornton JM. PROCHECK: a program to check the stereochemical quality of protein structures. J Appl Crystallogr 1993;26:283–291.
38. Georgescu RE, Alexov EG, Gunner MR. Combining conformational flexibility and continuum electrostatics for calculating pK(a)s in proteins. Biophys J 2002;83:1731–1748. [PubMed: 12324397]
39. Gilson MK, Honig B. Calculation of the total electrostatic energy of a macromolecular system: solvation energies, binding energies, and conformational analysis. Proteins 1988;4:7–18. [PubMed: 3186692]
40. Huang J, Lipscomb WN. T-state active site of aspartate transcarba- mylase: crystal structure of the carbamyl phosphate and L-alanosine ligated enzyme. Biochemistry 2006;45:346–352. [PubMed: 16401065]
41. Jin L, Stec B, Kantrowitz ER. A cis-proline to alanine mutant of *E. coli* aspartate transcarbamoylase: kinetic studies and three-dimensional structure. Biochemistry 2000;39:8058–8066. [PubMed: 10891088]
42. Stieglitz K, Stec B, Baker DP, Kantrowitz ER. Monitoring the transi- tion from the T to the R state in E. coli aspartate transcarbamoylase by X-ray crystallography: crystal structures of the E50A mutant in four distinct allosteric states. J Mol Biol 2004;341:853–868. [PubMed: 15288791]
43. Pettersen EF, Goddard TD, Huang CC, Couch GS, Greenblatt DM, Meng EC, Ferrin TE. UCSF chimera—a visualization system for exploratory research and analysis. J Comput Chem 2004;25:1605–1612. [PubMed: 15264254]
44. DeLano, WL. The PyMol molecular graphics system. Palo Alto, California, USA: DeLano Scientific; 2002 [Accessed on 15 Jan 2006]. Available at: http://www.pymol.org
45. Corder TS, Wild JR. Discrimination between nucleotide effector responses of aspartate transcarbamoylase due to a singe site substitution in the allosteric binding site. J Biol Chem 1989;264:7425–7430. [PubMed: 2651439]
46. Stieglitz KA, Dusinberre KJ, Cardia JP, Tsuruta H, Kantrowitz ER. Structure of the E. coli aspartate transcarbamoylase trapped in the middle of the catalytic cycle. J Mol Biol 2005;352:478–486. [PubMed: 16120448]
47. Williams MK, Stec B, Kantrowitz ER. A single mutation in the reg- ulatory chain of Escherichia coli aspartate transcarbamoylase is an extreme T-state structure. J Mol Biol 1998;281:121–134. [PubMed: 9680480]
48. Robey EA, Wente SR, Markby DW, Flint A, Yang YR, Schachman HK. Effect of amino acid substitutions on the catalytic and regulatory properties of aspartate transcarbamoylase. Proc Natl Acad Sci USA 1986;83:5935–5938.
49. Stebbins JW, Robertson DE, Roberts MF, Stevens RC, Lipscomb WN, Kantrowitz ER. Arginine 54 in the active site of Escherichia coli aspartate transcarbamoylase is critical for catalysis: a site-specific mutagenesis, NMR and X-ray crystallographic study. Protein Sci 1992;1:1435–1446. [PubMed: 1303763]
50. Stebbins JW, Xu W, Kantrowitz ER. Three residues involved in binding and catalysis in the carbamyl phosphate binding site of Escherichia coli aspartate transcarbamylase. Biochemistry 1989;28:2592–2600. [PubMed: 2659074]

51. Macol C, Dutta M, Stec B, Kantrowitz ER. The 80s loop of the cat- alytic chain of Escherichia coli aspartate transcarbamoylase is critical for catalysis and homotropic cooperativity. Protein Sci 1999;8:1305–1313. [PubMed: 10386880]

52. Bruns CM, Hubatsch I, Ridderstrom M, Mannervik B, Tainer JA. Human glutathione transferase A4-4 crystal structures and mutagenesis reveal the basis of high catalytic efficiency with toxic lipid peroxidation products. J Mol Biol 1999;288:427–439. [PubMed: 10329152]

53. Fenn TD, Ringe D, Petsko GA. POVScript1: a program for model and data visualization using persistence of vision ray-tracing. J Appl Crystallogr 2003;36:944–947.

54. Baker NA, Sept D, Joseph S, Holst MJ, McCammon JA. Electrostatics of nanosystems: application to microtubules and the ribosome. Proc Natl Acad Sci USA 2001;98:10037–10041. [PubMed: 11517324]

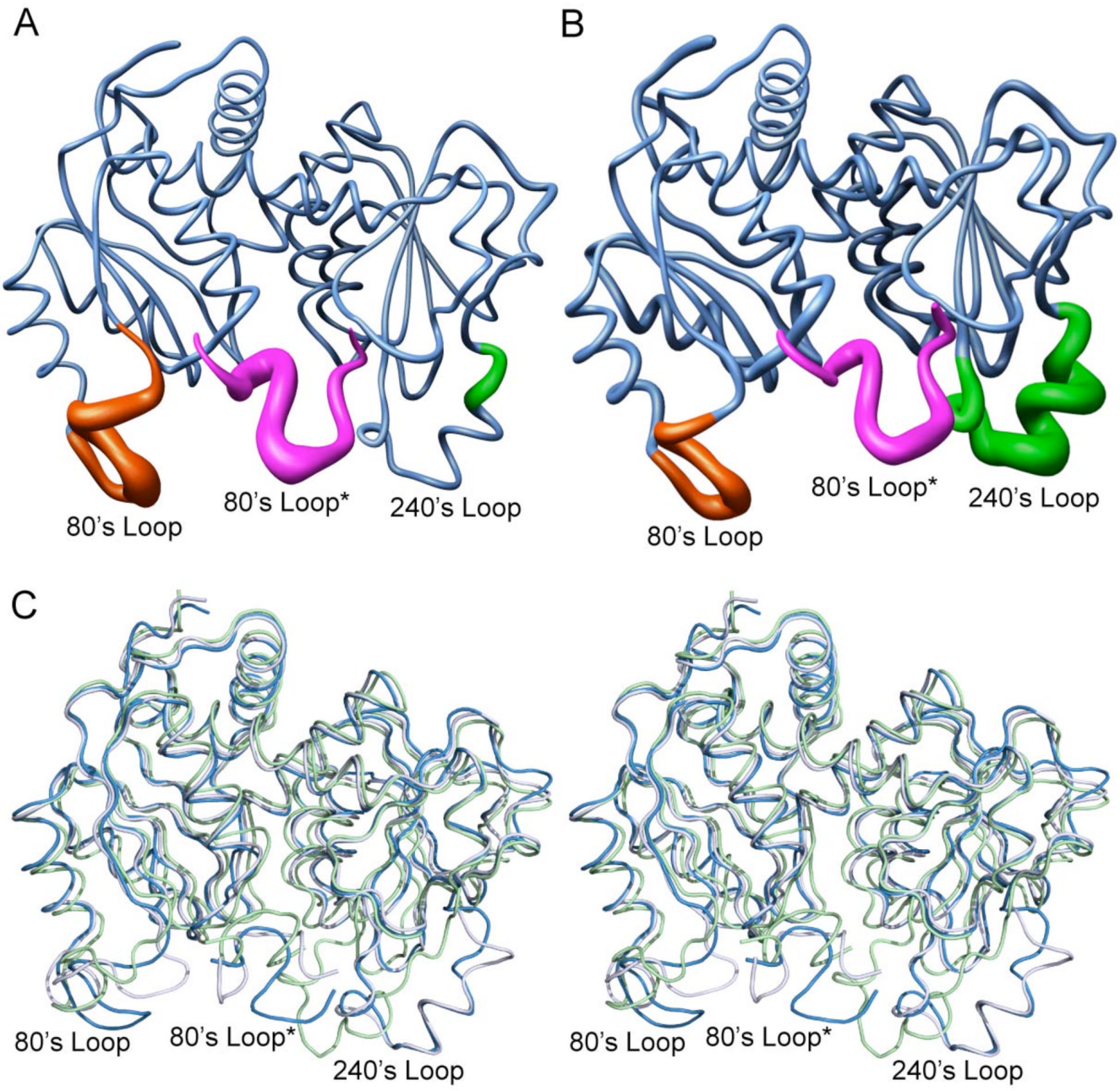

Figure 1.

A: Comparison of the C1 chain and the 80's loop of the C2 chain of the T_{high_apo} with corresponding portions of the T_{low_apo} structure. B: Comparison of the C1 chain and the 80's loop of the C2 chain of the T_{high_apo} with corresponding portions of the R_{low_pala} structure. The width of the tube is proportional to the RMS deviation of the a-carbon atom positions. Also shown is the 80's loop from the adjacent catalytic chain that contributes residues to the active site (80's Loop*). C: Stereoview of a superposition of the a-carbon atoms of the T_{high_apo} (blue), T_{low_apo} (gray), and the R_{low_pala} (green) structures. Parts A and B were prepared using CHIMERA,[43] whereas Part C was prepared using PyMol.44

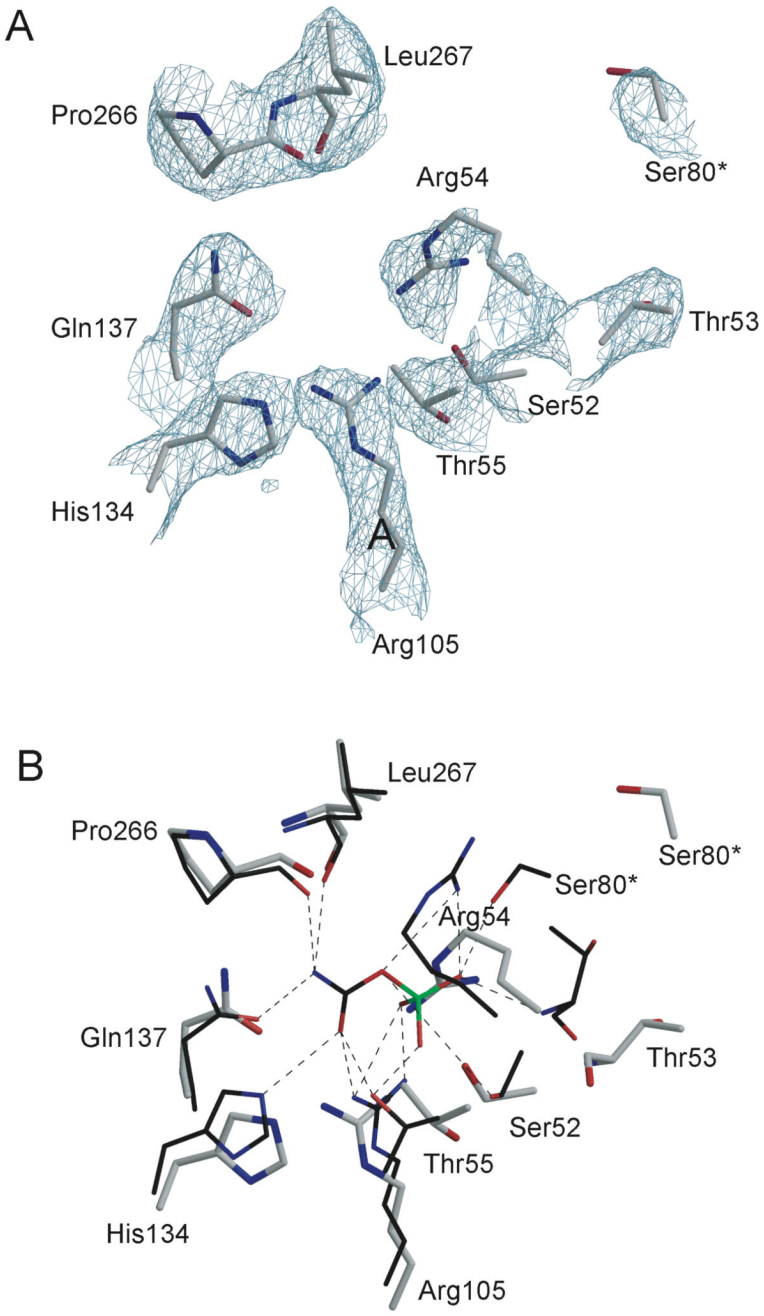

Figure 2.

A: The 2Fo - Fc electronic density map of active site of the T_{high_apo} structure contoured at 1.8σ with the refined coordinates overlaid. B: Overlay of active site of the T_{high_apo} structure (gray) and the $T_{low\_CTP\_CP}$ structure (black). The interactions between the CP and enzyme in the $T_{low\_CTP\_CP}$ structure are shown as dotted lines. Superposition of the structures was performed using SEQUOIA[46] and the figure was prepared with POVScript1.[47]

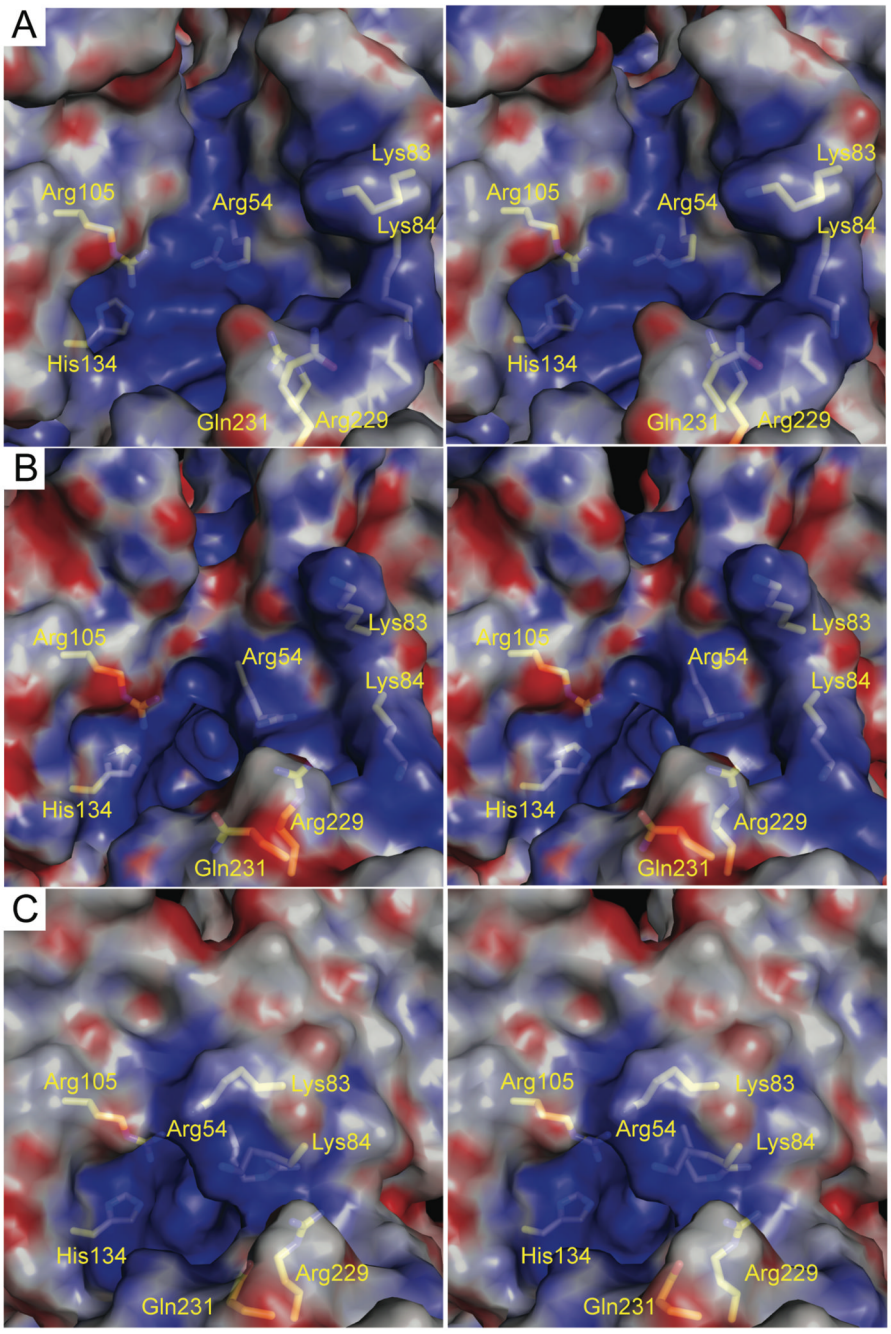

Figure 3.

Electrostatic potentials mapped on the molecular surface of active site of the **(A)** T_{high_apo} structure, **(B)** T_{low_apo} structure, and **(C)** $T_{low\_CTP\_CP}$ structure in the range ±15 kT/e. The positions of Arg54, His134, Arg105, Arg229, and Gln231 and Lys83 and Lys84 from the adjacent chain are shown. Electrostatic potentials were calculated using APBS.[48] The dielectric of the protein and the solvent were set to 4 and 80, respectively. This figure was prepared with PyMol[44] and the APBS tools plug-in employing standard charges on the amino acid side chains except for those indicated in Table II. For these amino acids the charges were calculated at pH 7 using the indicated pK_a values in Table II.

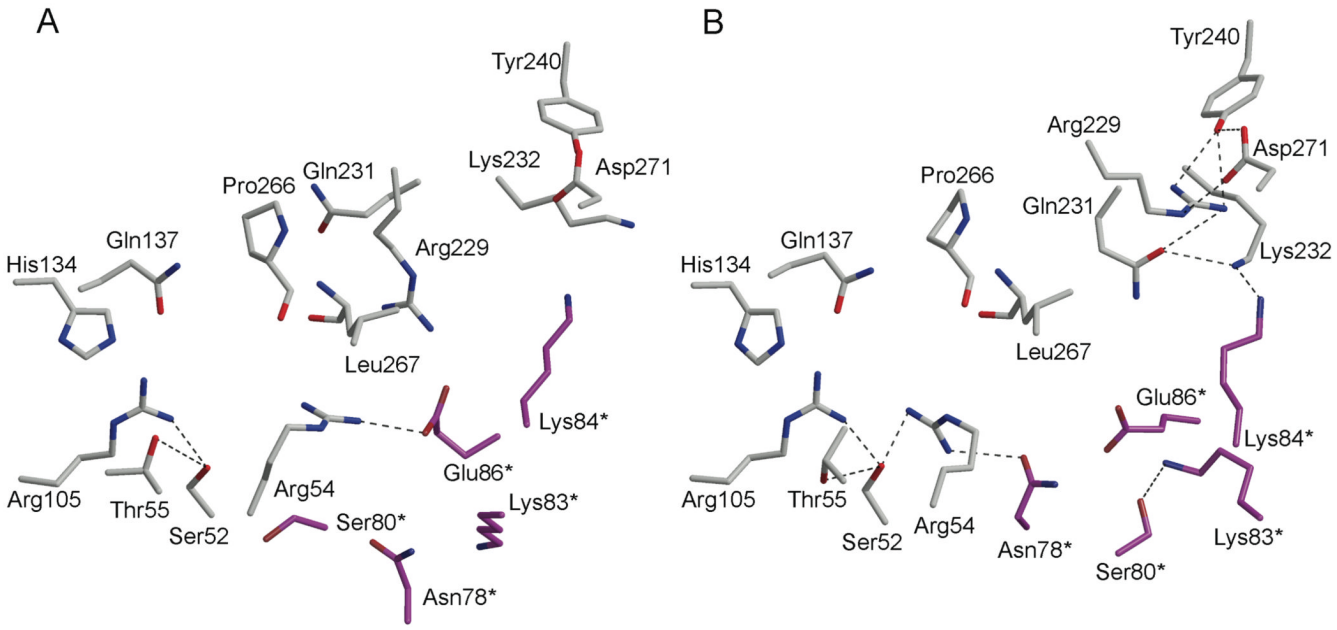

Figure 4.

The active site architecture of the (A) T_{low_apo} and (B) T_{high_apo} structures. Residues from C1 chain are in gray and residues from C2 chain are in magenta. An asterisk after the residue number indicates it is from the C2 chain. This figure was drawn with POVScript1.[47]

Table I

X-ray Data Collection and Refinement statistics for the ATCase pH 8.5 Structure

Data collection		
Space Group	H3	
Cell Dimensions:		
	a = *b*, *c* (Å)	129.78, 197.74
	α, β, γ (°)	90, 90, 120
Resolution (Å)	50.00−2.80	
Rmerge[a](%)	0.106 (0.329)	
Average (I/σ)	5.8 (2.1)	
Completeness (%)	99.7 (99.0)	
Total Reflections	102,066	
Unique reflections	27,528	
Redundancy	3.71 (3.45)	
Refinement		
Resolution (Å)	50.00−2.80	
Reflections	80,493	
R_{factor}/R_{free}	0.215/0.247	
RMS deviations:		
Bonds (Å)	0.014	
Angles (°)	0.83	
Mean B value (Å^2)	40.8	
Total number waters	213	

Values in parentheses are for the highest resolution shell

a

$$R_{merge} = \frac{\sum |I_{hkl} - \overline{I_{hkl}}|}{\sum \overline{I_{hkl}}}$$

Table II

Comparison of calculated pK_a values for side chains in the T_{low_apo} and T_{high_apo} structures. See the Methods and Materials section for details of the pK_a calculations that were done using MCCE. Only these residues which had ΔpK_a values greater than one are shown.

Side Chain pK_a Values			
Residue	**T_{low_apo}**	**T_{high_apo}**	**ΔpK_a**
Lys84c2	10.8	8.7	2.5
Lys232c1	10.0	11.9	1.9
His134c1	5.8	7.6	1.8
Glu86c2	5.0	8.5	3.5